

Article

Comparison of Measurement Protocols for Internal Channels of Transparent Microfluidic Devices

Joris Kaal¹, Nicolas Feltin², Marc Lelong², Huabing Yin³ , Andrew Glidle³, Kevin Romieu⁴ 
and Elsa Batista^{5,*} 

- ¹ CEA-Leti, Commissariat à l'Énergie Atomique et aux Énergies Alternatives, Université Grenoble Alpes, F-38000 Grenoble, France; joris.kaal@cea.fr
- ² Laboratoire National de Métrologie et d'Essais-Nanometrology, CEDEX, 78197 Trappes, France; nicolas.feltin@lne.fr (N.F.); marc.lelong@lne.fr (M.L.)
- ³ Division of Biomedical Engineering, School of Engineering, University of Glasgow, Glasgow G12 8LT, UK; huabing.yin@glasgow.ac.uk (H.Y.); andrew.glidle@glasgow.ac.uk (A.G.)
- ⁴ CETIAT, Centre Technique des Industries Aérouniques et Thermiques, F-69603 Villeurbanne, France; kevin.romieu@cetiat.fr
- ⁵ Metrology Department, Portuguese Institute for Quality (IPQ), 2829-513 Caparica, Portugal
- * Correspondence: ebatista@ipq.pt; Tel.: +351-212948167

Abstract: The microfluidic industry faces a significant challenge due to the lack of sensitive and standardized methods. One critical need is the measurement of internal channel dimensions in fully assembled chips. This study presents and compares several protocols for measuring these dimensions, including optical profilometry, optical microscopy, and tiled digital imagery. Standardized chips made from two materials commonly used in microfluidics (borosilicate glass and Cyclic Olefin Copolymer) were evaluated using each protocol. A consistency analysis using normalized error statistics identified optical profilometry as the most reliable method, offering the lowest uncertainty and the highest consistency with nominal geometry values. However, all protocols encountered difficulties with vertical depth measurements of internal structures. Future research should focus on addressing these limitations, including investigating the influence of multiple refractive surfaces on optical profilometry and exploring confocal microscopy. In conclusion, this work provides a comprehensive comparison of measurement protocols for internal microfluidic structures and offers a practical solution for applications in the microfluidic industry, while also identifying important directions for future research.



Academic Editors: Michele Norgia, Rahul Kumar and Han Haitjema

Received: 2 September 2024

Revised: 4 December 2024

Accepted: 6 January 2025

Published: 10 January 2025

Citation: Kaal, J.; Feltin, N.; Lelong, M.; Yin, H.; Glidle, A.; Romieu, K.; Batista, E. Comparison of Measurement Protocols for Internal Channels of Transparent Microfluidic Devices. *Metrology* **2025**, *5*, 4. <https://doi.org/10.3390/metrology5010004>

Copyright: © 2025 by the authors. Licensee MDPI, Basel, Switzerland. This article is an open access article distributed under the terms and conditions of the Creative Commons Attribution (CC BY) license (<https://creativecommons.org/licenses/by/4.0/>).

Keywords: microfluidic chips; optical measurements; channels dimensions; methods validation

1. Introduction

Microfluidics has long held the potential to disrupt a wide range of fields [1–3]. Aiming at the miniaturization of analytical and chemical methods [4], microfluidics continues to promise revolutionary advancements across many industries [5].

In recent years, the microfluidics industry has experienced remarkable growth, driven by applications such as chemical analysis, point-of-care diagnostics [6,7], and pharmaceutical research [8,9], including microphysiological systems [10,11]. The growth is projected to continue at a compound annual growth rate of 2.2% until 2028 [12].

Regardless of the application, the internal geometry of microfluidic channels is often crucial to the functionality of the device. For example, point-of-care diagnostic devices required precise dilution ratios, while microphysiological systems need physiologically

relevant shear stresses [13,14], both of which impose strict geometrical constraints on chip manufacturers.

Given the importance of the internal geometry to a device's functionality, it is crucial for the industry to be able to accurately characterize the internal dimensions of a chip. Microfluidic chips are often made of multiple structured layers that are sealed together to form the final product. While measuring the dimensions of the structure before assembly is feasible (for example, using optical microscopy or stylus profilometry), once sealed, the channels are encapsulated inside the chip. This makes their characterization more difficult due to material properties and physical constraints. This issue is significant because the assembly process can change the structure of the chip compared to its pre-assembled state, leaving both the manufacturer and the user uncertain about the actual geometry and dimensions of the flow circuit in use.

The industry itself has identified the lack of sensitive and standardized testing methods as one of the major hurdles preventing microfluidics from fulfilling its promises [15,16]. To help address this challenge, this work presents multiple protocols for measuring the internal dimensions of fully assembled transparent chips. The reproducibility and precision of each protocol are analyzed and compared. Both glass and polymer chips are used as substrates to evaluate the influence of material on measurement reproducibility.

The protocols described in this study enable automated, non-destructive, reproducible characterization of the internal geometry of transparent microfluidic chips after assembly, making them suitable for industrial applications. By removing the uncertainty caused by potential deformation during assembly, these protocols ensure that users can trust the devices they are using, and manufacturers can be confident in the quality of the chips they are providing.

Here, we describe the chip designs and different measuring techniques. The different sets of results are analyzed through consistency tests between the protocols and nominal values. Finally, we examined the influence of two different materials on dimension measurements.

2. Chips Geometries

Batches of chips were designed and manufactured using two different materials: D263©bio glass [17] (a common type of borosilicate glass) and COC (Cyclic Olefin Copolymer, tradename TOPAS© [18]). The chips made from each material have different internal dimensions and designs. The choice of geometries was based on different applications for these chips within the EURAMET 20NRM02 MFMET project [19] (MFMET—Establishing Metrology Standards in Microfluidic devices [20]). These tests mainly include leakage tests [21], flow resistivity tests [22], and the dimensional measurements described here.

All designs adhere to the ISO 22916:2022 standard on interoperability requirements for dimensions, connections, and initial classification of microfluidic devices [23]. This standard has a notable influence on the chips' footprint, as well as the positions and dimensions of their connections. This allows different participants to use the same connector and be confident that the chips were compatible with each other's measurement setup. In addition, these chips are intended to serve as transfer standards for other laboratories. By adhering to ISO 22916:2022, compatibility with laboratories outside the scope of this project will also be facilitated.

2.1. Glass Transfer Standard Chips

Eight designs (footprint 15 mm × 45 mm) were developed for glass chips (see Figure 1). Each design has one or several main channels, with some connected to one or multiple "leakage channels"—these are significantly smaller in cross-section compared to the main

channels, simulating a leak. All designs, except Design 08, include a reference channel (Channel 01 in Figure 1) that does not have any additional side channels. Figure 2 shows an example of Design 04 chips. Technical design drawings of these glass transfer standard chips are available in the Electronic Supplementary Information.

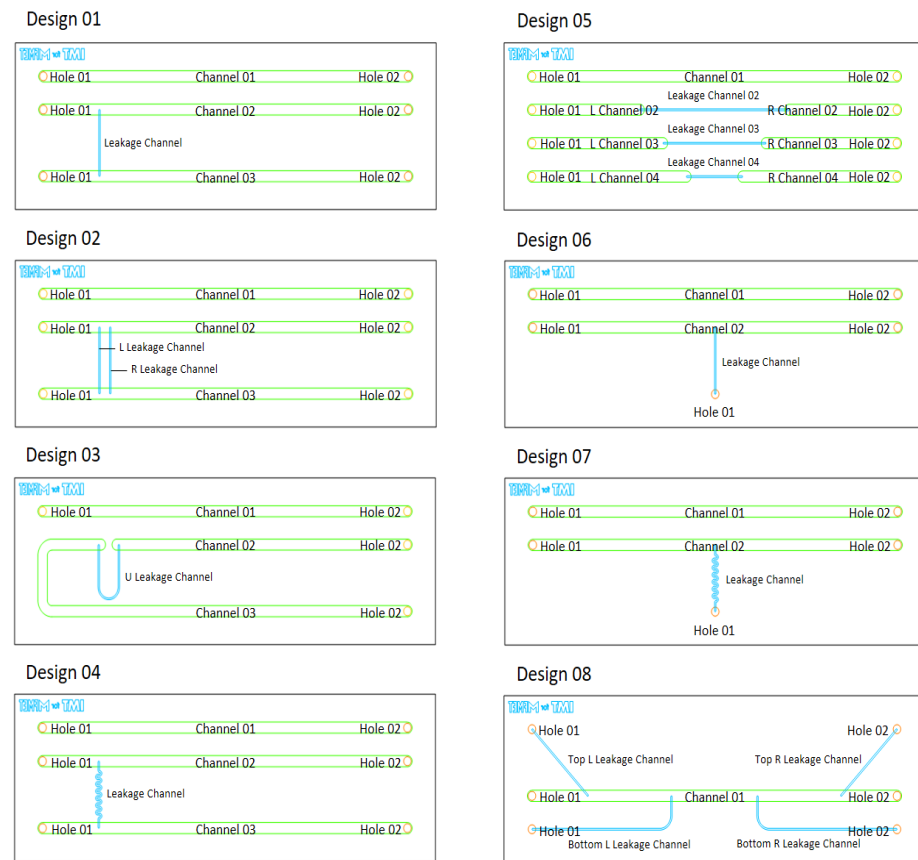


Figure 1. Different glass chip designs and their geometry nomenclature for measurements.



Figure 2. Example of a glass transfer standard chip, Design 04.

The glass chips were fabricated by IMT Masken und Teilungen AG, Greifensee, Switzerland, using D263©bio glass [17], via isotropic wet-etching techniques, employing hydrofluoric acid-based etching solutions commonly used in the semiconductor industry. The final chips consist of two halves that were individually fabricated and then bonded together. The critical dimensions of the device were verified during and after processing for quality assurance. For Designs 01 to 05, four chips were produced, while Design 06 and 07 had three chips each, and Design 08 had two. One chip from each design was reserved as a backup.

2.2. Polymer Transfer Standard Chips

The polymer transfer standard chip has the same footprint as a standard microscope slide and contains eight different designs on a single chip (see Figure 3). Each design consisted of two main channels with a “leakage channel”. The leakage channels came in two distinct lengths: four designs had longer leakage channels, and the other four had shorter ones. The cross-section of the leakage channels is rectangular and varies between designs. Figure 4 shows an example of one of the polymer chips. Detailed designs, technical drawings, and CAD files of the polymer chip design can be found in the Electronic Supplementary Information.

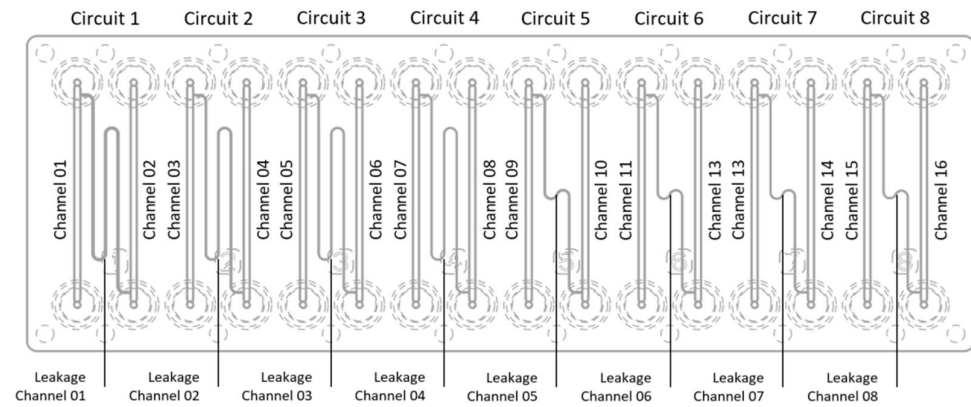


Figure 3. Polymer chip design and its geometry nomenclature for measurements.



Figure 4. Example of a polymer transfer standard chip.

The polymer chips were produced by microfluidic ChipShop GmbH, Jena, Germany, using injection molding.

Once the fabrication process is complete, the top part containing the microfluidic structure is sealed onto a thin bottom slide to close the chip. The entire chip is made of COC (Cyclic Olefin Copolymer, tradename TOPAS© [18]).

3. Three Different Measurement Protocols

The different pieces of equipment used for the measurement protocols set out below are shown in Figure 5, with specifications given in Table 1.

Table 1. Specifications of the different instruments used for dimension measurements.

Instrument	Lens	Lighting	Calibration	Uncertainty Linked to Calibration
OGP SmartScope ZIP®250	×1 ×2	Substage LED profile Coaxial LED surface SmartRing™ LED ring light	Annual calibration report by OGP	In plane (XY): ±2 µm + 4 L/1000 Vertically (Z): ±2.5 µm + 5 L/1000 In-image: <1 µm

Table 1. Cont.

Instrument	Lens	Lighting	Calibration	Uncertainty Linked to Calibration
Olympus BX53M	×1.5 ×5 ×15	Substage tungsten bulb lighting	Test pattern (see Figure 5)	0.1%
Leica Wild M3Z	×2.56	Overhead LED ring light	Test pattern (see Figure 5)	2%
Nikon D5300	×1, f/2.8, 105 mm macro lens	Fluorescent tube lighting below sample	Test pattern (see Figure 5)	In-image: 0.45% On tiled images: 0.76%
Zeiss AxioObserver	×2.5	Transmission lighting from quartz halogen bulb	Test pattern (see Figure 5)	0.15%

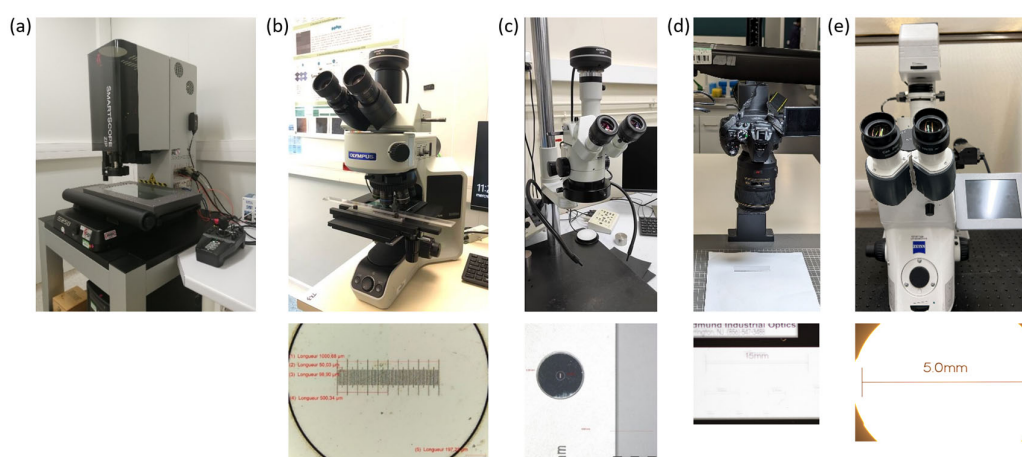


Figure 5. The different setups used for dimension measurements. (a) Optical profilometer OGP SmartScope ZIP®250. (b) Optical microscope Olympus BX53M with its calibration gauge. (c) Stereo binocular microscope Leica Wild M3Z with its calibration gauge. (d) Digital camera Nikon D5300 with its calibration gauge. (e) Optical microscope Zeiss AxioObserver with its calibration gauge.

Examples of the optical images obtained from each of the techniques are given in Figure 6, together with details showing which points in the images were used as reference criteria from which the measurement values were obtained.

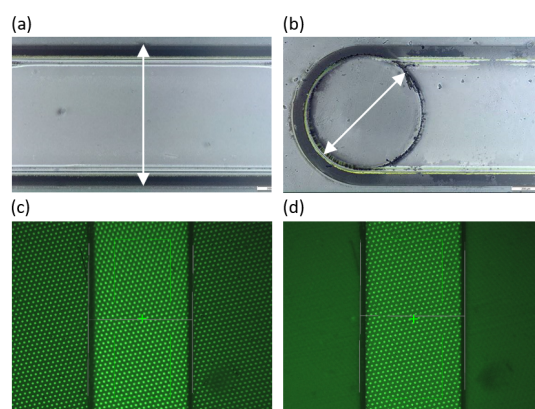


Figure 6. Cont.

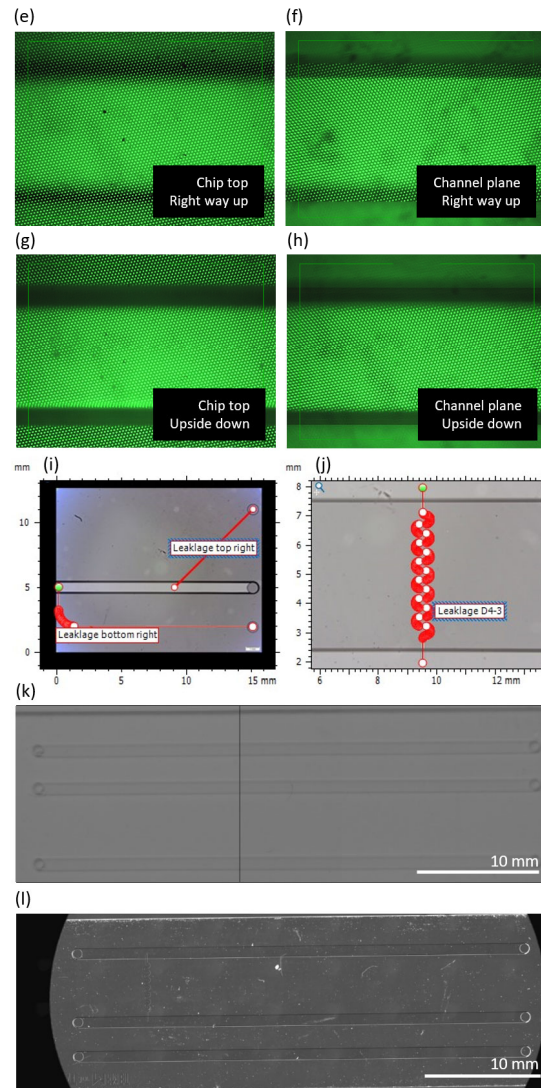


Figure 6. Definition of measurement points (images (b–h) from the Optical Profiler; (i) from the Leica Wild M3Z; (j) from the Olympus BX53M; (k) from the Nikon D5300; and (l) from the Zeiss AxioObserver). (a) The width of the channels is taken as the maximum width. (b) The diameter of the holes is measured by recognizing the internal hole features. (c) Point at the bottom Z-plane of the polymer channel. (d) Point at the top Z-plane of the polymer channel. (e) Point at the top plane of the glass chip when the chip is the right way up (see Section 3.1). (f) Point at the measurable channel plane of the glass chip when the chip is the right way up. (g) Point at the top plane of the glass chip when the chip is upside down (see Section 3.1). (h) Point at the measurable channel plane of the glass chip when the chip is upside down. (i) MountainsMap’s “Distance between two points” and “Customized path” tools applied to Design 08. (j) MountainsMap’s “Distance between two points” and “Customized path” tools applied to S-channel in design 04. (k) A stitched image of Design 01 created using the Nikon D5300 camera. (l) A stitched image of Design 04 created using the Zeiss AxioObserver with Ludl BioPoint2 stage showing the ability to discern the leakage channel (left hand side of image) when using higher NA optics.

3.1. Protocol 1: Optical Profilometry

The first protocol entails optical profilometry, a method that uses light instead of a physical probe to characterize geometries. This allows non-destructive measurements without direct contact with the object, making it particularly suitable for transparent substrates.

A SmartScope ZIP[®]250 (with its accompanying software, ZONE3[®], both from Optical Gaging Products (OGP), part of Quality Vision International (QVI), Rochester, NY, USA)

was used to perform measurements of the internal geometries. Table 1 gives details of the instrument, and the setup is shown in Figure 5a.

The instrument is annually recalibrated by OGP staff, ensuring the accuracy shown in Table 1 (Calibration report available in the Electronic Supplementary Information). It is important to note the difference in uncertainty between measurements where the stage moves a distance, L , between two measured points and static in-image measurements.

The OGP SmartScope ZIP[®]250 can automatically focus on a plane within a user-defined margin. The software identifies geometrical features from the focused image and measures the dimension of interest. For example, to determine the width of a channel, the profilometer finds the focus plane at the top of the channel, identifies the outermost edges, and measures the width between these edges (see Figure 6).

Depth measurements proved to be more challenging, particularly in glass compared to polymer chips. For polymer chips, the depths of all channels were measured by determining focus planes at the top and bottom of the channel using the software's "Focus" tool, which establishes a 3D point on each plane. The software then calculates the channel depth by measuring the distance in Z-axis between these two points (Figure 6).

However, depth measurements inside transparent materials using optical profilometry are subject to distortion due to the material's refractive index, which depends on both material and the wavelength of light used to determine the focus plane. The SmartScope ZIP[®]250 uses grid light with a wavelength range from 575 nm to 625 nm. For polymer chips, a refractive index (RI) of $n_D = 1.53$ for 589 nm at 25 °C (provided by microfluidic ChipShop GmbH, Germany) was used to correct for the difference between and optical path length and physical distance measurement [24]; thus, all depth measurements in polymer chips were multiplied by n_D .

For glass, the optical profilometer struggled to differentiate between the focus planes at the top and bottom of the channels. Therefore, a more complex approach was used to estimate the channel depth. The profilometer could determine the top and bottom planes of the chip and one plane of the channel (Figure 6). The assumption was made that this plane belonged to the upper channel. In this method, when the chip is right-side up, the top of the chip, the top of the channel, and the bottom of the chip are measured. When the chip is flipped upside down, the bottom of the chip, the bottom of the channel, and the top of the chip are measured. The following formula was then used to estimate the depth of the channel:

$$D = ((z_{chnl,2} - z_{top,2}) - (z_{chnl,1} - z_{top,1})) \cdot n_D \quad (1)$$

where D is the estimated channel depth; $z_{-(chnl,2)}$ and $z_{-(top,2)}$ are the z -coordinates of the measurable channel plane and the top plane measured when the chip is upside down; $z_{-(top,1)}$ and $z_{-(chnl,1)}$ are the z -coordinates of the measurable channel plane and the top plane measured when the chip is right-side up; and n_D is the refractive index of D263©bio glass. Based on the OGP light wavelength range, a refractive index = 1.5230 for 589.2938 nm [25], provided by Schott AG, Germany, was used to correct for RI effects [17].

The length of the main channels was defined as the maximum distance between the inlet and outlet hole centers. Hole diameters were determined using the "Feature finder" tool, which measures the internal circumference of the holes (Figure 6). Leakage channel lengths were measured using start and end reference points taken from the mid-point of a line drawn across the intersection of the leakage channel with the wall of a main channel.

Measuring the lengths of more complex, non-linear channels (such as L-, U-, and S-shaped channels) posed difficulties. Despite multiple attempts using different settings and ZONE3© tools, no reproducible parameters were found.

All the above steps are programmable on the OGP SmartScope ZIP[®]250. This allows a specific measurement protocol—including positions, fields of view, focus zones, lighting,

and image processing settings—to be stored and repeated for identical objects. Once established, the measurement program was run three times on each chip.

Using the data from each run, an average and a standard deviation (s_r) were determined. Together with the uncertainty from the instrument's calibration (u_c), noted in Table 1, the standard uncertainty (u) of the measurement was calculated using the following formula:

$$u = \sqrt{u_c^2 + s_r^2} \quad (2)$$

The calculation assumes that these are the two largest sources of uncertainty. For the purpose of this article, variability in the refractive index was not considered, which could be investigated in future research.

3.2. Protocol 2: Optical Microscopy

The second protocol uses standard optical microscopy. Depending on the size of the microfluidic geometries, two different microscopes were employed: an optical microscope (Olympus BX53M) or a stereo binocular microscope (Leica Wild M3Z) was used. Details of both instruments are provided in Table 1.

Each instrument has its own calibration gauge structure (Figure 5), ensuring that measurement results are traceable to the International System of Units (SI). The uncertainties associated with the calibration of each instrument can be found in Table 1.

The width and length of the leakage channels, the width of the main channels, and the diameters of the holes were all measured using the Olympus BX53M (with the $\times 5$ or $\times 10$ lens). Images were taken and analyzed using Olympus Stream Essentials 2.3.3 (Build 17023). This software has the capability to continuously capture images and automatically detect different focal planes, creating a merged image where measurements were made.

Similar to the optical profilometer in Protocol 1, the largest dimension was used to define the channel width (Figure 6). The length of the main channels was measured as the maximum distance between the inlet and outlet holes, using the Leica Wild M3Z binocular microscope. The focal plane was manually adjusted for these measurements.

For hole diameter measurements, a circle tool was used. However, identifying the correct focal plane was difficult, as multiple focal planes were closely spaced. It was hypothesized to be due to the hole-drilling process during chip manufacturing. Several measurements were performed, and an uncertainty value was assigned to take into account the various focal planes and irregularities in the structure.

The length of non-linear channels (both main and leakage channels) was measured using specific tools from the MountainsMap© version 10 software package (from Digital Surf, France). Depending on the channel shape's complexity, either the "Distance between two points" tool or the "Customized path" tool was used (Figure 6). In both cases, the length was determined along the median line of the channel width.

As with Protocol 1, each chip was measured three times, and the results were used to calculate a standard uncertainty using the same approach.

3.3. Protocol 3: Tiled Digital Imagery

The third protocol uses two different instruments, both with a wide field of view: a Nikon D5300 digital camera fitted with a 105 mm, $1\times$, $f/2.8$ macro lens; and a Zeiss AxioObserver optical microscope equipped with a Ludl BioPoint2 motorized stage, Zeiss EC Plan Neofluar $2.5\times/0.085$ objective, and Zeiss HRc camera. Details of both devices are included in Table 1.

Digital cameras, such as the Nikon D5300, offer portability, affordability, and high resolution. Since they can detect events within entire microfluidic devices, they have been widely used with paper-microfluidic devices for on-site diagnosis [26,27] and high-speed

imaging and detection of events within microfluidic devices [28]. The Zeiss AxioObserver, similar to the microscope used in Protocol 2, provides more precise measurements.

Both instruments were calibrated using standard reference bars (Figure 6), which allowed for the determination of the resolution of the instruments and the uncertainty linked to calibration (Table 1). The calibration report is available in the Electronic Supplementary Information.

In this protocol, measurements were made using image processing. For hole diameters and channel widths, both instruments could produce results from a single image. The uncertainty in these measurements was based solely on the consistency associated with the instruments' calibration.

For measuring the lengths of the main channels, tiled images were used. The number of frames needed to cover the entire microfluidic channel depended on the field of view of the instrument. The accuracy of the measurement was affected by how well the frames were stitched together, the quality of images, and the uncertainty linked to the instrument's calibration.

The Nikon D5300 camera, with its large field of view, required only two frames to cover an entire main channel in the glass chips (see Figure 6 for an example). The images were taken with overlapping areas such that they could be stitched together in ImageJ by overlaying blemishes in successive frames. The uncertainty from stitching was 3 pixels/frame (1 pixel = 8.44 μm according to calibration). Due to the lower image quality, there was a significant uncertainty in defining the ends of the channels. This was approximately 6 pixels at each end, resulting in a total uncertainty of 15 pixels, which equals 0.31% of the total length of 39,800 μm . Furthermore, the leakage channels were not sufficiently visible in the images, making accurate measurements unreliable. Including the instrument uncertainty (0.45%; see Table 1), the potential total uncertainty for length measurements using this system was 0.76%.

The Zeiss AxioObserver, equipped with a motorized Ludl BioPoint2 stage, also used stitched images (see Figure 6 for an example). However, the precision and reproducibility of the Ludl BioPoint2 stage (<1 μm) were sufficient, so the results were highly consistent. The main advantage of this instrument was the higher numerical aperture (NA) of the 2.5 \times objective (NA = 0.085), which gave clearer images. This improved clarity made it easier to define channel and hole borders, resulting in a notable improvement in measurement precision. Therefore, the uncertainty in defining the channel ends was negligible, with an error of at most 1 pixel. Hence, the total uncertainty for the length measurements using the Zeiss AxioObserver was the same as its in-image uncertainty from calibration (i.e., 0.15%; see Table 1).

Both instruments were used to measure multiple glass chips, and the average of multiple measurements from each method was taken as final value. Given this combination of two different methods, the standard uncertainty definition from Equation (2) needs to be updated as follows:

$$u = \sqrt{u_{c1}^2 + u_{c2}^2 + s_r^2} \quad (3)$$

where u_{c1} is the standard uncertainty associated with the Nikon D5300 (which differs between in-image and tiled-image measurements, as shown in Table 1), u_{c2} is the uncertainty associated with the calibration of the Zeiss AxioObserver, and s_r remains the standard deviation between the two values.

3.4. Evaluation of the Measurement Results

To evaluate the consistency of the three protocols, their results are compared against a reference value. For each measurement (for example the diameter of Hole 01 in Channel 01 of Design 01), a reference value can be defined. This reference value (called RV) is

determined as the mean of the measurement values from the three protocols combined, using the weighted means formula. The inverse square of the standard uncertainty (u_n) associated with the average of a protocol's measurement values (x_n) serves as its weighting factor [29]:

$$RV = \frac{x_1/u^2(x_1) + \dots + x_n/u^2(x_n)}{1/u^2(x_1) + \dots + 1/u^2(x_n)} \quad (4)$$

The following formula gives the standard uncertainty, $u(RV)$, associated with the reference value [29]:

$$u(RV) = \sqrt{\frac{1}{\frac{1}{u^2(x_1)} + \dots + \frac{1}{u^2(x_n)}}} \quad (5)$$

Once the reference value and its standard uncertainty are determined, the measurement values from each protocol can be tested for consistency with this reference value. To identify this consistency, the normalized error (E_n) is calculated [30]:

$$E_n = \frac{x_n - RV}{\sqrt{U^2(x_n) - U^2(RV)}} \quad (6)$$

where E_n is a protocol's consistency indicator for a specific measurement; x_n is the average of a protocol's measurement values; RV is the reference value of the same measurement; and $U(x_n)$ and $U(RV)$ are their associated expanded uncertainties, calculated as $U = k \times u$ with $k = 2$.

The value of E_n leads to the following conclusions:

- If $|E_n| \leq 1$, the protocol's measurement values are consistent for a certain measurement (test passed).
- If $|E_n| > 1$, the protocol's measurement values are inconsistent for a certain measurement (test failed).

This approach allows for a comparison of the protocols between each other. However, it does not necessarily indicate the accuracy of all protocols. Besides a reference value, a nominal value can also be defined for all measurements. These nominal values and their standard uncertainties are based on the design drawings with quality assurance measurements and statistical tolerances provided by IMT Masken und Teilungen AG. The nominal values represent the theoretical dimensions that the geometry should have.

For the diameters of the holes, no statistical data were available, so the nominal value from the design (i.e., 800 μm) was used. Based on IMT's experience, a standard uncertainty of 15 μm was assumed, resulting in an expanded uncertainty of 30 μm .

The depth was measured by IMT during quality assurance, with values falling within a range of (98.3 ± 0.4) μm , giving an expanded uncertainty of 0.8 μm .

The width of the main channels was estimated using the known depth, leading to a calculated nominal width of (996.6 ± 2.66) μm for this specific batch of chips.

Finally, the length of the main channels, defined as the maximum distance between the inlet and outlet holes (designed at 39,800 μm), depends on the precision of hole placement. Based on IMT's experience, a precision of 7.5 μm per hole was assumed, leading to a total standard uncertainty of 15 μm for the length of the main channels and, thus, an expanded uncertainty of 30 μm .

Using these estimations, the consistency of the measurement values of each protocol with the nominal values can be tested.

To investigate the influence of material on measurements, a straightforward approach was adopted. Protocol 1 was applied to both glass and polymer chips, and the standard uncertainty of the measurements was compared. This standard uncertainty, defined in Equation (2), consists of a standard deviation term (s_r), related to the actual measurements,

and an uncertainty term (u_c), related to the calibration of the machine used. Since the calibration uncertainty for the OGP SmartScope ZIP[®]250 is identical for both polymer and glass measurements, it is more informative to compare the standard deviations of the actual measurements. Thus, the standard deviations from Protocol 1 for both polymer and glass measurements will be compared.

4. Results

4.1. Glass Chips

Each protocol naturally gave a set of results for the glass chips. The three complete sets of results can be found in the Electronic Supplementary Information. For analysis purposes, the results from a single chip, Design 01—series 01, and only its first channel, Channel 01, will be treated here. In this channel, the protocols performed the following measurements:

- The diameter of Hole 01;
- The diameter of Hole 02;
- The width of the channel;
- The depth of the channel;
- The length of the channel.

The subsequent figures (Figures 7–11) show the resulting values from all three protocols, their associated reference value, and the nominal value of each measurement.

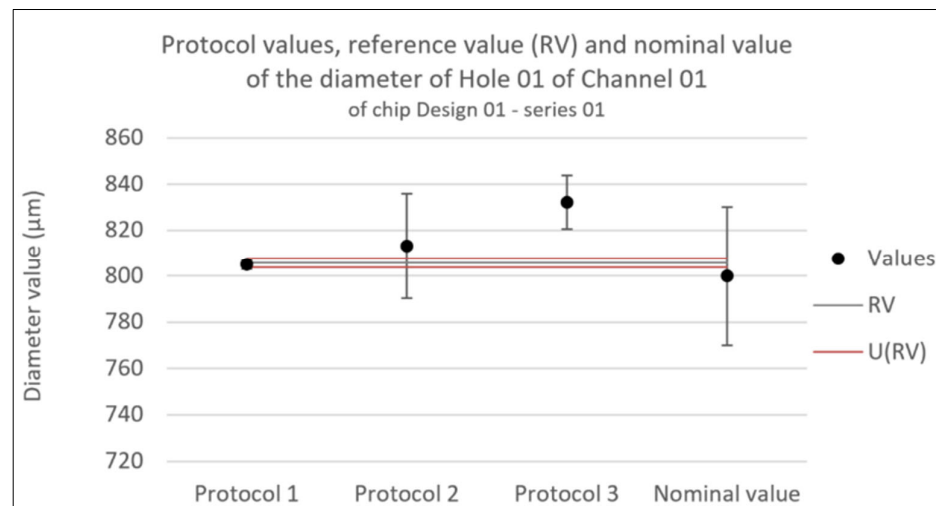


Figure 7. Consistency test for the diameter of Hole 01 in Channel 01 of chip Design 01—series 01. Error bars represent the expanded uncertainty. Likewise, U(RV) is the expanded uncertainty associated with the reference value.

To determine the consistency between the different protocols and their resulting reference value, the normalized error values (E_D) are shown in Table 2.

Table 2. Normalized error values between protocols and their resulting reference value (RV) for each measurement. Values that indicate inconsistency are marked in red.

	Diameter Hole 01	Diameter Hole 02	Width	Depth	Length
Protocol 1	−1.78	−4.44	−1.57	N/A	1.48
Protocol 2	0.33	4.14	1.65	N/A	0.32
Protocol 3	2.30	1.12	−0.40	N/A	−1.95

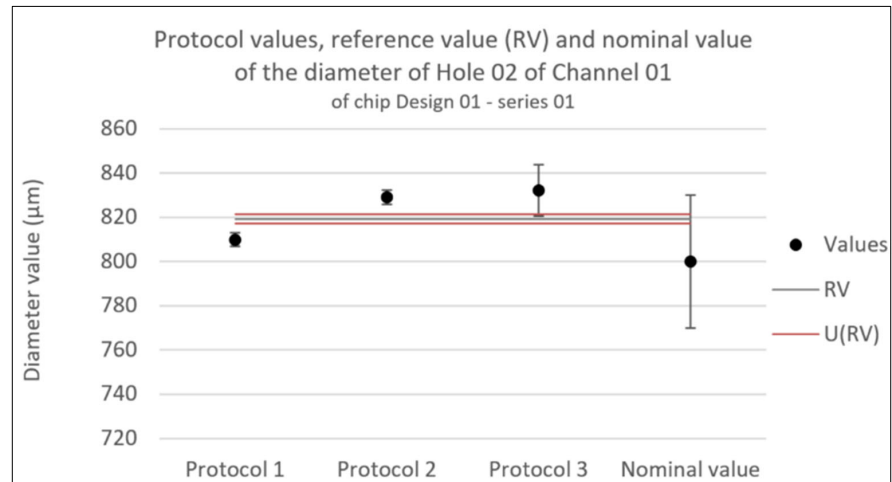


Figure 8. Consistency test for the diameter of Hole 01 in Channel 01 of chip Design 01—series 01. Error bars represent the expanded uncertainty. Likewise, U(RV) is the expanded uncertainty associated with the reference value.

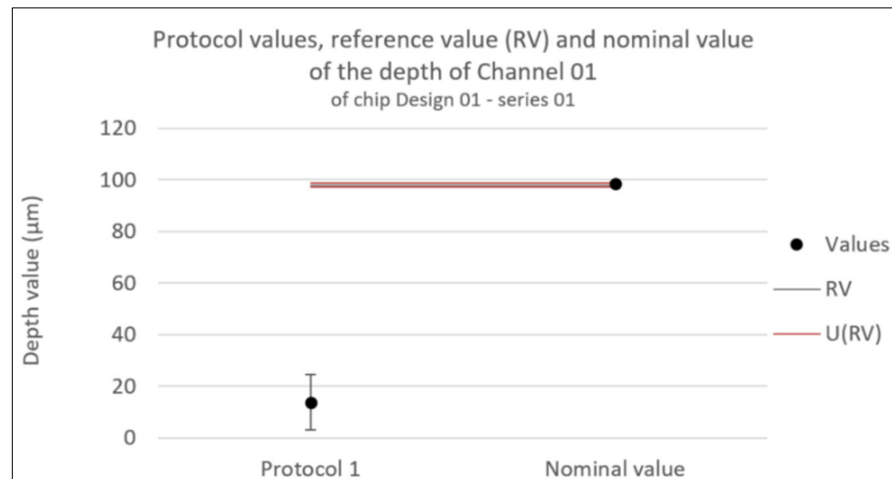


Figure 9. Consistency test for the depth of Channel 01 of chip Design 01—series 01. Error bars represent the expanded uncertainty. Likewise, U(RV) is the expanded uncertainty associated with the reference value.

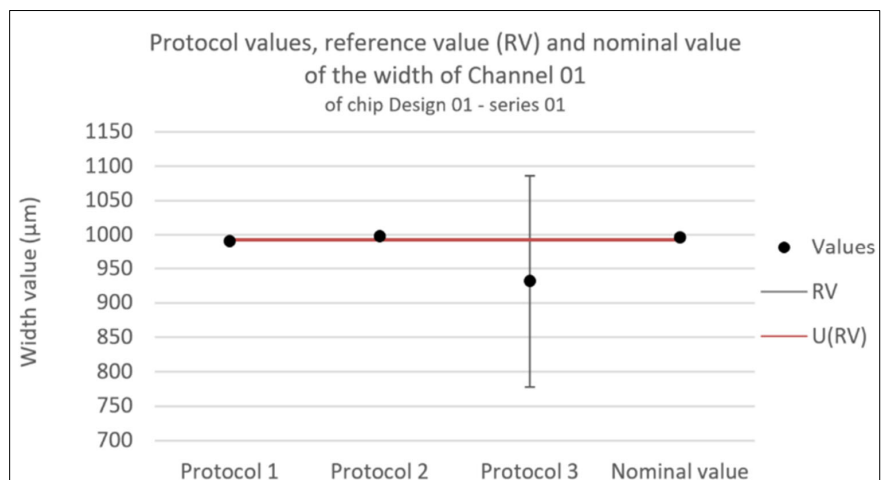


Figure 10. Consistency test for the width of Channel 01 of chip Design 01—series 01. Error bars represent the expanded uncertainty. Likewise, U(RV) is the expanded uncertainty associated with the reference value.

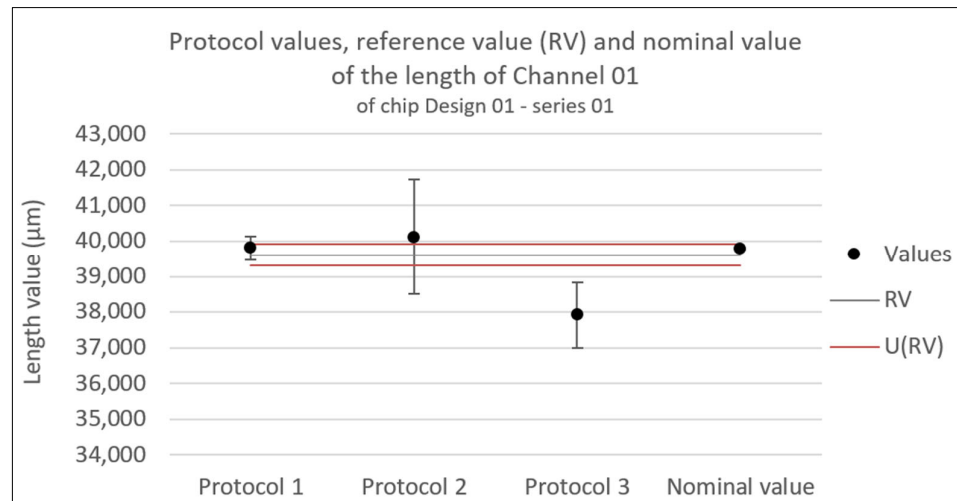


Figure 11. Consistency test for the length of Channel 01 of chip Design 01—series 01. Error bars represent the expanded uncertainty. Likewise, U(RV) is the expanded uncertainty associated with the reference value.

Given that the depth was only measured with Protocol 1, there is no reference value or normalized error for a consistency test.

Finally, the consistency between the protocols and the nominal value was determined for each measurement. The normalized errors for this consistency test are shown in Table 3.

Table 3. Normalized error values between protocols and the nominal value for each measurement. Values that indicate inconsistency are marked in red.

	Diameter Hole 01	Diameter Hole 02	Width	Depth	Length
Protocol 1	0.16	0.33	−0.93	−7.81	0.02
Protocol 2	0.35	0.96	0.23	N/A	0.20
Protocol 3	0.99	0.99	−0.42	N/A	−2.04

4.2. Polymer Chips

The full set of results from the polymer chips acquired with Protocol 1 can be found in the Electronic Supplementary Information. As an excerpt, Table 4 shows the width and depth measurements, as well as their standard deviations, for the first design of one of the COC chips. To facilitate a more meaningful comparison of these standard deviations against those from measurements made on glass chips, they are expressed in percentages.

Table 4. Measurements of the width and depth of the channels in Circuit 1 of one of the TOPAS© COC chips, as well as their associated standard deviations.

	Width		Depth	
	Average Measured	Standard Deviation	Average Measured	Standard Deviation
Channel 01	503.1 µm	0.1 µm (0.0%)	358.0 µm	1.7 µm (0.5%)
Leakage Channel 01	108.5 µm	0.1 µm (0.1%)	123.6 µm	1.8 µm (1.4%)
Channel 02	508.1 µm	0.1 µm (0.0%)	372.9 µm	2.7 µm (0.7%)

For comparison purposes, Table 5 provides measurements and uncertainties from Protocol 1 for the measurement directions corresponding to those of Table 4.

Table 5. Measurements of the width and depth of the channels of glass chip Design 01—series 01, as well as their associated standard deviations.

	Width		Depth	
	Average Measured	Standard Deviation	Average Measured	Standard Deviation
Channel 01	991.3 μm	0.2 μm (0.0%)	13.8 μm	4.6 μm (33.0%)
Channel 02	992.1 μm	0.2 μm (0.0%)	17.9 μm	1.3 μm (7.6%)
Channel 03	992.4 μm	0.2 μm (0.0%)	20.2 μm	3.3 μm (16.3%)
Leakage channel	143.0 μm	0.5 μm (0.3%)	N/A	N/A

5. Discussion

5.1. Comparison of Protocols

The normalized error values in Table 2 suggest that the protocols are often inconsistent with the reference values. On the contrary, Table 3 shows the protocols mostly consistent with the nominal values. The consistency of Protocol 1 with the nominal values slightly outperforms that of Protocol 2, which in turn slightly outperforms Protocol 3. This implies while the different protocols produce different values, they remain consistent with the nominal values and their expanded uncertainties. This also indicates the need for a more detailed exportation of the uncertainty calculations, as they are likely underestimated across all protocols.

In particular, for longer dimensions, such as the channel length, the accuracy of the optical profilometer is higher than that of the other protocols.

Several factors may explain the decreased accuracy of the length measurements in Protocol 3. The most evident reason is the extra uncertainty term introduced in the standard uncertainty definition due to the combination of two different methods (see the comparison between Equation (2) to Equation (3)). Additionally, the uncertainty of each method includes an extra factor related to image stitching, on top of the uncertainty associated with calibration. Lastly, the average and standard deviations for Protocol 3 are based on two measurement points, one from each method. Improving any of these three factors might potentially improve the consistency of this protocol with the nominal values for length.

In terms of uncertainty, Protocol 1 presents smaller values than the others in all measurement dimensions.

5.2. Close-Up on Depth Measurements

For the depth measurements shown in Figure 10, only Protocol 1 was capable of providing results, but these were inconsistent with the nominal values (see Table 3 and, additionally, Table 5). Several factors could explain this inconsistency and suggest potential improvements.

First, the measurements were corrected with the refractive index of the material. The refractive index is given for a specific wavelength (589 nm), which may not exactly match the wavelength of the SmartScope ZIP[®]250 used in Protocol 1. OGP indicated that the wavelength of the grid light for measurements in Z could range from 575 to 625 nm (Table 6).

However, even if the wavelength is different slightly, considering the material's refractive index variations, it is unlikely to cause significant changes in the measured values [17,25].

Table 6. Refractive indices of D263©bio glass for different wavelengths spanning the SmartScope.

n_C (643.8469 nm) ZIP [®] 250 focus light range.	1.5209
n_D (589.2938 nm)	1.5230
n_e (546.074 nm)	1.5255 ± 0.0015

If the value of the refractive index is not the issue, then it may be the method of applying it. The straightforward multiplication of the measured values with the refractive index to correct for deformation is regularly used for structures with a single refractive interface. However, for an internal channel with two refractive interfaces, this assumption might not hold, and further investigation is warranted, which would also take into account the NA of the imaging optic and its influence on the estimated optical path length.

Another possibility is that the optical profilometer did not accurately measure either of the two surfaces. Given the high surface quality of wet-etched channels and the proximity of its top and bottom planes, the channel itself might act as a lens. In this case, the low surface roughness, which is usually considered an advantage, might impede proper measurement. This too would be worth further investigation.

It seems unrealistic to hypothesize that the bonding process has altered the channel depth from the quality assurance value of $98.3 \pm 0.4 \mu\text{m}$ to the measured values in Table 5. A destructive test could verify this; however, other tests performed on these chips within the 20NRM02 MFMET project would likely have detected such a drastic geometry change.

To suggest further improvements in depth measurement for internal microfluidic channels, an additional method was tested. The following paragraph describes preliminary results obtained during this work, which could provide an interesting avenue for future work on depth measurement protocols for internal microfluidic channels.

Leakage Channel 02 of a polymer chip was measured using a Zeiss LSM 510 confocal fluorescence microscope. The instrument operates based on a confocal principle, which eliminates out-of-focus light from focal planes (called optical sections) and collects serial optical sections. In comparison to conventional epifluorescence microscopy, confocal microscopy can produce three-dimensional images by stacking up a series of Z-images. Confocal microscopy is well suited to measure the depth of an enclosed microfluidic channel. It must be noted that a fluorophore solution was injected into the chip for these measurements.

The obtainable resolution in Z depends on the NA value and the magnification of the microscope's objectives. Two objectives were used: an $\times 20$ NA = 0.5 objective and an $\times 100$ NA = 1.3 objective, allowing for a resolution in Z of $2.07 \mu\text{m}$ and $0.44 \mu\text{m}$, respectively. The higher NA value objective thus enables thinner optical slicing. With this objective, however, for optical sections further away from the base of the channel, the fluorescence intensity significantly decreases because of fluorescence self-absorption effects. This effect is clearly visible in Figure 12.

Figures 13 and 14 show the resulting Z-stacks of the confocal fluorescence measurements made with the $\times 20$ NA = 0.5 objective and the $\times 100$ NA = 1.3 objective, respectively.

To estimate the channel height using these confocal measurements, first it is necessary to determine the sections at which the fluorescence intensity in the channel is significant compared to outside the channel. This can be performed by comparing the intensity at the center of the channel to the intensity measured outside of the channel (as shown in Figure 12).

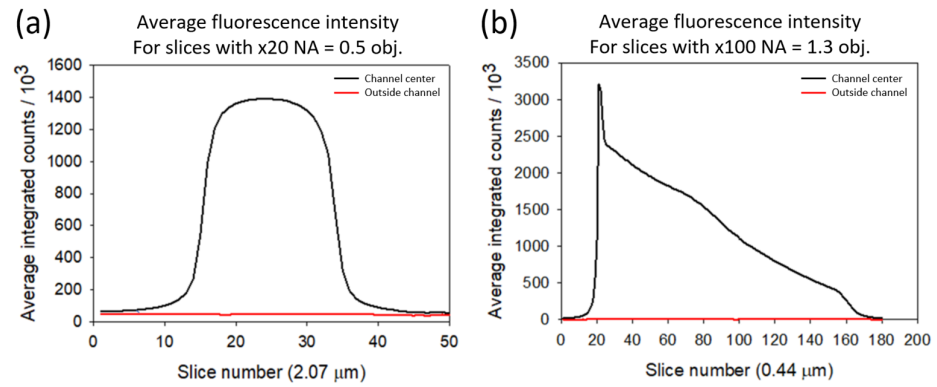


Figure 12. Average fluorescence intensity for successive optical sections (slices) measured in the center of the channel (black) and to the side of the channel (red). Base of the channel at slice 0. (a) Measurements from the $\times 20$ NA = 0.5 objective, $2.07 \mu\text{m}$ sections. (b) Measurements from the $\times 100$ NA = 1.3 objective, $0.44 \mu\text{m}$ sections.

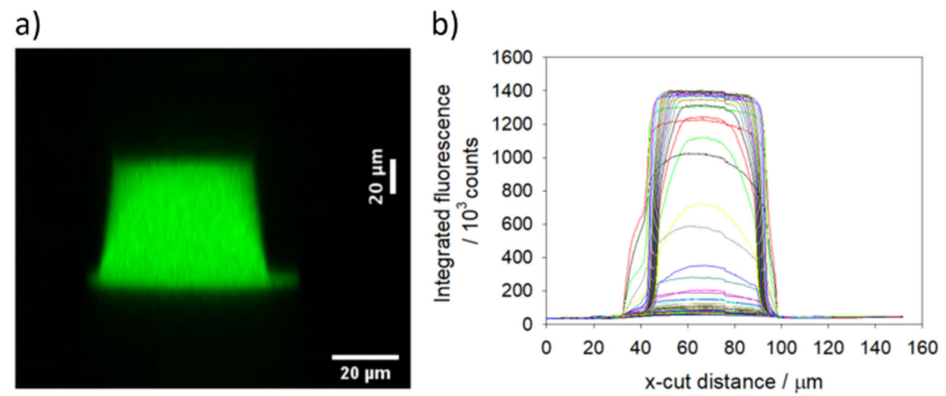


Figure 13. Integrated fluorescence intensity from Z-stack of all 50 optical sections taken with the $\times 20$ NA = 0.5 objective. (a) Cross-section of channel height. (b) Fluorescence Intensity profile of all optical sections over an x-cut perpendicular to both the long channel axis and the channel height axis.

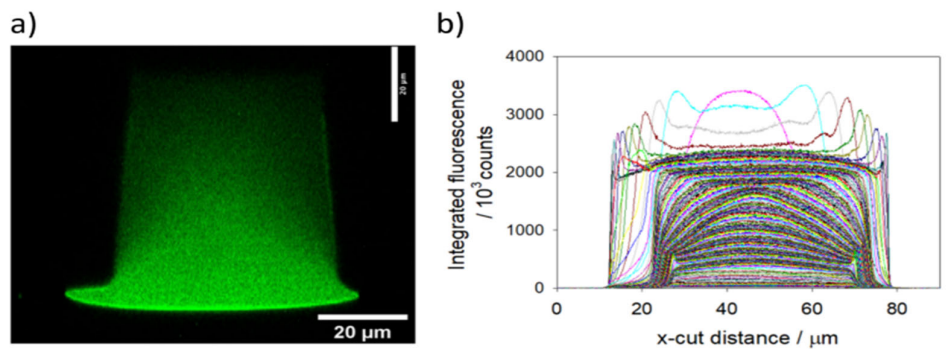


Figure 14. Integrated fluorescence intensity from Z-stack of all 180 optical sections taken with the $\times 100$ NA = 1.3 objective. (a) Cross-section of channel height. (b) Fluorescence Intensity profile of all optical sections over an x-cut perpendicular to both the long channel axis and the channel height axis.

Secondly, a decision needs to be made about the minimum value of fluorescence intensity within an optical section corresponds to that confocal slice being substantially within the channel. This decision is necessary because the confocality is not perfect: for all practical pinhole sizes, light from a range of Z-distances will pass through. For a homogeneous fluorescence solution, such as the one in use here, a lower limit for fluorescence intensity to determine whether an optical section is substantially within the channel could, for example, be taken as 1% of that found at the channel’s mid-height.

Using this 1% criteria, it is possible to estimate that 37 of the 50 optical sections from the $\times 20$ NA = 0.5 objective are substantially within the channel. With its resolution in Z of $2.07\ \mu\text{m}$ (calibrated to be accurate to $0.1\ \mu\text{m}$ using an internal encoder), the channel height of the polymer device is estimated at $(74.5 \pm 4)\ \mu\text{m}$ (there will be at least one slice uncertainty at both the top and bottom of the channel).

Despite the fact that the profiles collected using the $\times 100$ NA = 1.3 objective appear noisy (especially at sections further from the channel base), it is possible to make an accurate estimate of which slices have a fluorescence intensity above the 1% threshold. For the $\times 100$ NA = 1.3 objective, there are 166 out of 180 optical sections above the 1% fluorescence intensity criteria, corresponding to a channel height estimate of $(73.0 \pm 0.8)\ \mu\text{m}$.

Thus, the two measurements are consistent with each other, with the $\times 100$ NA = 1.3 objective having greater precision.

There is a channel height discrepancy between the design specifications and the height measured by confocal microscopy. These parts are made by sealing an upper piece, which bears the imprinted channel profile, to a lower piece that is a plain (flat) plastic substrate. A significant fraction of this discrepancy in heights is most likely due to the bonding process used to seal the two pieces together. As can be seen from the fluorescence x-cut profiles of Figures 13 and 14, the measured width of the lowest 5–10 μm of the channel is significantly larger than the main part of the channel (at approximately 30 μm above the base). If this lower, wider part of the channel profile is disregarded, and the fluorescence criteria used to define the channel height is relaxed from 1% to 5% of the main channel intensity, then the measurement of upper piece channel height becomes 56 μm , significantly closer to the design specification of 50 μm .

These preliminary results hint in the direction of another interesting method worth investigating in future work for depth measurements of internal channels in transparent microfluidic devices.

5.3. The Influence of Different Materials

Following the comparison between protocols, the influence of different materials on measurements will be considered. Measurements taken on polymer and glass chips in the XY-plane will be considered separately from those taken in the Z-axis.

The standard deviations in the XY-plane (width measurements from Tables 4 and 5) are generally within the range of a few tenths of micrometers for both polymer and glass measurements. When expressed as percentages, it becomes even more evident that the standard deviation is negligible for both materials.

It would be interesting for future research to investigate whether this observation holds true for other materials commonly used in microfluidics (e.g., PP, PC, COP, and PMMA) and other measurement methods (e.g., optical or confocal microscopy). Experience suggests that the SmartScope ZIP[®]250's apparent indifference to material type may not necessarily be extended to other techniques.

In contrast, the standard deviations of the depth measurements in TOPAS[®] COC are much lower than those for D263[®]bio glass.

During the measurements, it was noticed that the SmartScope ZIP[®]250 seemed to distinguish more clearly between the top and bottom planes of the internal channels in the polymer chips. For this reason, the Z-coordinates of the top and the bottom planes were subtracted directly to calculate the channel depth. As mentioned earlier, it is hypothesized that the polymer chips' higher surface roughness, which is usually a disadvantage, might have helped the optical profilometer better define a focus plane compared to the near-perfect smoothness of the wet-etched glass channels. Testing this hypothesis would be an interesting avenue for future research.

It is worth noting that, regardless of whether the standard deviation is low or high, the accuracy of depth measurements in both materials is questionable. In both TOPAS® COC and D263®bio glass, the depth measurements were inconsistent with their nominal values. In addition, although the profilometer was seemingly capable of distinguishing between the top and bottom of the internal channels in the polymer chips, it is difficult to differentiate it from the actual bottom of the chip. This might explain the overestimation of the depth of Leakage Channel 01, as shown in Table 4.

6. Conclusions

Accurately measuring internal structures after chip assembly is a well-recognized challenge in the microfluidic industry. This study, conducted as part of the EMPIR MFMET project, compared three different protocols, namely optical profilometry, optical microscopy, and tiled digital imagery, for measuring different internal microfluidic structures in chips made from D263®bio glass and TOPAS® COC.

A consistency analysis using normalized error statistics revealed Protocol 1, optical profilometry, as the preferred method due to its low uncertainty compared to the other protocols and its higher consistency with nominal geometry values.

However, challenges were encountered in measuring the depth of the internal geometries. The only protocol able to provide a measurement of the internal channel depth, optical profilometry, gave results that are highly inconsistent with their nominal values. Several avenues for future research are proposed, including a study of how to apply the refractive index for deformation compensation when dealing with multiple refraction interfaces. Another promising method is confocal fluorescence microscopy, which showed promising preliminary results.

The performance of TOPAS® COC chips was not significantly better or worse than that of D263®bio glass chips. This suggests that both materials are equally compatible with optical profilometry. However, depth measurements presented an exception, as channels with poorer surface roughness were easier to measure using the optical profilometer. Despite that, the depth measurements for the TOPAS® COC chips were also unsatisfactory. Further research comparing other common materials in microfluidics and different measurement techniques is recommended.

The results of this work directly address the current lack of accurate, robust, and validated measurement methods for internal microfluidic structures, offering a comprehensive comparison of different protocols and ultimately suggesting a preferred option for immediate application in the microfluidic industry. Additionally, this study offers valuable directions for future research, taking an important step toward overcoming a significant challenge that has hindered the microfluidic industry from reaching its full potential. The information obtained in this work also indicates the need for standardization in the field of dimensional measurements in microfluidic technology, especially after the chip's assembly. New European standardization projects will help in the development of standards for microfluidic dimension application within ISO/TC48/WG4 microfluidic devices, as foreseen in their new roadmap.

Supplementary Materials: The following supporting information can be downloaded at: <https://www.mdpi.com/article/10.3390/metrology5010004/s1>, Table S1: Glass Measurements Analysis; Table S2: Glass measurements for Analysis; Table S3: Glass Measurements protocol 1 CEA; Table S4: Glass Measurements protocol 2 LNE; Table S5: Glass Measurements protocol 3 UofG; Table S6: Polymer Measurements protocol 1 CEA; File S1: ChipDesign GlassTransferStandard IMT; File S2: ChipDesign PolymerTransferStandard MCS (pdf); File S3: ChipDesign PolymerTransferStandard MCS (stp); File S4: Calibration Report protocol1 CEA; File S5: Calibration Report protocol3 UofG.

Author Contributions: E.B. and K.R. were responsible for the conceptualization and supervision of the study. J.K. performed investigations of Protocol 1, defining its methodology and providing the required resources. N.F. did the same for Protocol 2, with assistance with the investigations from M.L., as did H.Y. for Protocol 3 and the confocal microscopy assisted in the investigations by A.G. Formal analysis of all results was performed by E.B. and J.K. The original draft was written by J.K., starting with input from E.B., H.Y. and N.F. for their respective parts. All authors have read and agreed to the published version of the manuscript.

Funding: This project 20NRM02 MFMET has received funding from the EMPIR programme co-financed by the Participating States and from the European Union’s Horizon 2020 Research and Innovation Programme.

Data Availability Statement: The original data presented in the study are openly available on the Zenodo repository Establishing Metrology Standards in Microfluidic Devices at <https://doi.org/10.5281/zenodo.11621010> (accessed on 4 December 2024).

Acknowledgments: This study is part of the work performed in the MFMET project. The authors recognize the contribution of all project participants and thank them for it. Secondly, the authors would like to express their gratitude to IMT Masken und Teilungen AG, Switzerland, and microfluidic ChipShop GmbH, Germany, for their contribution to the project, including but not limited to the development of the transfer standard chips used in this work. Finally, the authors want to thank all academic and industrial partners for continuously providing insights into microfluidic challenges and needs through discussions, workshops, or surveys conducted by The Microfluidics Association.

Conflicts of Interest: The authors declare no conflicts of interest.

References

1. Whitesides, G.M. The origins and the future of microfluidics. *Nature* **2006**, *442*, 368–373. [[CrossRef](#)] [[PubMed](#)]
2. Sackmann, E.K.; Fulton, A.L.; Beebe, D.J. The present and future role of microfluidics in biomedical research. *Nature* **2014**, *507*, 181–189. [[CrossRef](#)] [[PubMed](#)]
3. Elvira, K.S.; i Solvas, X.C.; Wootton, R.C.; Demello, A.J. The past, present and potential for microfluidic reactor technology in chemical synthesis. *Nat. Chem.* **2013**, *5*, 905–915. [[CrossRef](#)] [[PubMed](#)]
4. Berlanda, S.F.; Breitfeld, M.; Dietsche, C.L.; Dittrich, P.S. Recent Advances in Microfluidic Technology for Bioanalysis and Diagnostics. *Anal. Chem.* **2021**, *93*, 311–331. [[CrossRef](#)] [[PubMed](#)]
5. Convery, N.; Gadegaard, N. 30 years of microfluidics. *Micro Nano Eng.* **2019**, *2*, 76–91. [[CrossRef](#)]
6. Rosen, Y.; Gurman, P. MEMS and microfluidics for diagnostics devices. *Curr. Pharm. Biotechnol.* **2010**, *11*, 366–375. [[CrossRef](#)] [[PubMed](#)]
7. Behera, P.P.; Kumar, N.; Kumari, M.; Kumar, S.; Mondal, P.K.; Arun, R.K. Integrated microfluidic devices for point-of-care detection of bio-analytes and disease. *Sens. Diagn.* **2023**, *2*, 1437–1459. [[CrossRef](#)]
8. Huh, D.; Leslie, D.C.; Matthews, B.D.; Fraser, J.P.; Jurek, S.; Hamilton, G.A.; Thorneloe, K.S.; McAlexander, M.A.; Ingber, D.E. A Human Disease Model of Drug Toxicity–Induced Pulmonary Edema in a Lung-on-a-Chip Microdevice. *Sci. Transl. Med.* **2012**, *4*, 159ra147. [[CrossRef](#)] [[PubMed](#)]
9. Levner, D.; Ewart, L. Integrating Liver-Chip data into pharmaceutical decision-making processes. *Expert Opin. Drug Discov.* **2023**, *18*, 1313–1320. [[CrossRef](#)] [[PubMed](#)]
10. Quintard, C.; Tubbs, E.; Jonsson, G. A microfluidic platform integrating functional vascularized organoids-on-chip. *Nat. Commun.* **2024**, *15*, 1452. [[CrossRef](#)] [[PubMed](#)]
11. Middelkamp, H.; Weener, H.; Gensheimer, T.; van der Meer, A.D. Embedded macrophages induce intravascular coagulation in 3D blood vessel-on-chip. *Biomed. Devices* **2023**, *26*, 2. [[CrossRef](#)] [[PubMed](#)]
12. Yole Intelligence. *Status of the Microfluidics Industry 2023 Maturity of Microfluidics Devices Applications*; Yole Intelligence: Lyon, France, 2023.
13. Wang, K.; Man, K.; Liu, J.; Chen, Q.; Zhou, Y.; Yang, Y. Microphysiological Systems: Design, Fabrication, and Applications. *ACS Biomater. Sci. Eng.* **2020**, *6*, 3231–3257. [[CrossRef](#)] [[PubMed](#)]
14. Kim, H.; Lee, J.B.; Kim, K.; Sung, G.Y. Hydrophobic Sponge Structure–Based Triboelectric Nanogenerator. *J. Ind. Eng. Chem.* **2022**, *115*, 279–286. [[CrossRef](#)]

